



OPEN Transcriptome analysis in a humanized mouse model of familial dysautonomia reveals tissue-specific gene expression disruption in the peripheral nervous system

Ricardo HARRIPAUL^{1,2,3,4}, Elisabetta MORINI^{1,2,4}, Monica SALANI¹, Emily LOGAN¹, Emily KIRCHNER¹, Jessica BOLDOC¹, Anil CHEKURI^{1,2}, Benjamin CURRALL^{1,2,3}, Rachita YADAV^{1,2,3}, Serkan ERDIN^{1,3}, Michael E. TALKOWSKI^{1,2,3}, Dadi GAO^{1,2}✉ & Susan SLAUGENHAUPT^{1,2}✉

Familial dysautonomia (FD) is a rare recessive neurodevelopmental disease caused by a splice mutation in the Elongator acetyltransferase complex subunit 1 (*ELP1*) gene. This mutation results in a tissue-specific reduction of ELP1 protein, with the lowest levels in the central and peripheral nervous systems (CNS and PNS, respectively). FD patients exhibit complex neurological phenotypes due to the loss of sensory and autonomic neurons. Disease symptoms include decreased pain and temperature perception, impaired or absent myotatic reflexes, proprioceptive ataxia, and progressive retinal degeneration. While the involvement of the PNS in FD pathogenesis has been clearly recognized, the underlying mechanisms responsible for the preferential neuronal loss remain unknown. In this study, we aimed to elucidate the molecular mechanisms underlying FD by conducting a comprehensive transcriptome analysis of neuronal tissues from the phenotypic mouse model *TgFD9; Elp1^{Δ20/lox}*. This mouse recapitulates the same tissue-specific *ELP1* mis-splicing observed in patients while modeling many of the disease manifestations. Comparison of FD and control transcriptomes from dorsal root ganglion (DRG), trigeminal ganglion (TG), medulla (MED), cortex, and spinal cord (SC) showed significantly more differentially expressed genes (DEGs) in the PNS than the CNS. We then identified genes that were tightly co-expressed and functionally dependent on the level of full-length *ELP1* transcript. These genes, defined as *ELP1* dose-responsive genes, were combined with the DEGs to generate tissue-specific dysregulated FD signature genes and networks. Within the PNS networks, we observed direct connections between *Elp1* and genes involved in tRNA synthesis and genes related to amine metabolism and synaptic signaling. Importantly, transcriptomic dysregulation in PNS tissues exhibited enrichment for neuronal subtype markers associated with peptidergic nociceptors and myelinated sensory neurons, which are known to be affected in FD. In summary, this study has identified critical tissue-specific gene networks underlying the etiology of FD and provides new insights into the molecular basis of the disease.

Familial dysautonomia (FD) is a rare neurodevelopmental disorder that affects both the peripheral nervous system (PNS) and the central nervous system (CNS)¹. The underlying cause of FD is an intronic splice-site mutation in the Elongator acetyltransferase complex subunit 1 gene (*ELP1*, previously known as *IKBKAP*) that

¹Center for Genomic Medicine, Massachusetts General Hospital Research Institute, Boston, MA, USA. ²Department of Neurology, Massachusetts General Hospital and Harvard Medical School, Boston, MA, USA. ³Program in Medical and Population Genetics and Stanley Center for Psychiatric Research, Broad Institute of Harvard and MIT, Cambridge, MA, USA. ⁴These authors contributed equally: Ricardo HARRIPAUL and Elisabetta MORINI. ✉email: dgao2@mgh.harvard.edu; slaugenhaupt@mgh.harvard.edu

results in the tissue-specific skipping of exon 20². The nervous system expresses the lowest amount of full-length *ELP1* transcript and protein².

ELP1 encodes subunit 1 of the Elongator Acetyltransferase Complex, which is a highly conserved six-subunit complex^{3–8}. This complex is involved in numerous cellular functions, including exocytosis, cytoskeletal organization, axonal transport, cellular adhesion, cellular migration of cortical neurons, tRNA modification, and transcriptional elongation^{9–18}. Through its histone acetyltransferase activity, *ELP1* plays a significant role in transcriptional elongation and chromatin organization^{4,19,20}. *ELP1* also modulates translational efficiency with a biased usage of AA and AG-ending codons, through wobble uridine tRNA modifications^{21–23}.

FD patients exhibit a range of neurological symptoms that manifest from birth and worsen over time, including diminished pain and temperature sensation, visual loss, kyphoscoliosis, proprioceptive ataxia, and difficulty regulating body temperature and blood pressure^{1,24–26}. Loss of sensory neurons in the dorsal root ganglion (DRG), including nociceptors and proprioceptors, is a prominent feature of FD^{25,27–29}. Nociceptors are specialized sensory neurons that detect and transmit signals related to pain and temperature perception. In FD patients, there is a diminished ability to perceive pain and temperature, which can lead to insensitivity to potentially harmful stimuli³⁰. Proprioceptors are sensory neurons responsible for detecting body position and movement and their loss in FD results in proprioceptive ataxia, causing difficulties in coordinating movements and maintaining balance^{30,31}. The loss of both nociceptors and proprioceptors contributes to the complex neurological symptoms observed in FD patients.

Mouse models of FD have contributed significantly to our understanding of the role of *ELP1* in neural development and function. Multiple studies have provided evidence supporting the crucial role of *ELP1* in maintaining neuronal survival and tissue innervation^{32–34}. The *Elp1* KO mouse provided the first insights into the role of *Elp1* in transcriptional elongation and gene expression regulation despite leading to lethality at the mid-gastrulation stage⁷. RNA-seq transcriptomic profiling of mouse embryos expressing increasing levels of human *ELP1* revealed dysregulation of genes essential to early-stage nervous system development and to the identification of a set of co-expressed genes whose expression highly correlated with the level of *ELP1*³⁵. These *ELP1* dose-responsive genes were enriched for axon and cell projection formation which supports the role of *ELP1* in the expression of genes important for target tissue innervation and is consistent with the innervation failure observed in FD³⁵. A phenotypic FD mouse model was generated by introducing the human *ELP1* transgene carrying the FD major splice mutation (*TgFD9*) into a hypomorphic *Elp1* ^{Δ 20/*Flox*} mouse²⁷. This humanized mouse mimics the tissue-specific mis-splicing seen in FD patients, as well as many phenotypic characteristics of the human disease^{36,37}.

While the PNS is known to be significantly affected in FD, the specific gene networks responsible for this disruption have not been identified. In the current study, we uncovered putative, tissue-specific, and convergent molecular mechanisms underlying FD by analyzing the transcriptomes of several neuronal tissues (Fig. 1). We collected DRG and trigeminal ganglion (TG) as representative PNS tissues, and cortex, medulla (MED), and spinal cord (SC) as representative CNS tissues, from both control and FD phenotypic mice³⁶ (Fig. 1A). To unravel tissue-specific transcriptomic dysregulation, we identified differentially expressed genes (DEGs) and *ELP1* dose-responsive genes (Fig. 1A). We then constructed FD-dysregulated gene networks from these transcriptional signatures based on their known protein–protein interactions (Fig. 1B). Finally, we compared FD signature genes to determine functional convergence across tissues in FD (Fig. 1C). This comprehensive transcriptome analysis provides valuable insights into the regulatory mechanisms underlying FD pathogenesis and sheds light on the shared dysregulation observed in FD PNS tissue.

Results

ELP1 reduction leads to tissue-specific transcriptome changes

To uncover the tissue-specific molecular alterations underlying FD, we conducted transcriptome analysis in DRG, TG, cortex, MED, and SC from 3-month-old, humanized FD-phenotypic mouse *TgFD9; Elp1* ^{Δ 20/*Flox*}³⁶. The *TgFD9; Elp1* ^{Δ 20/*Flox*} mouse carries one *Elp1* allele in which exon 20 is deleted (*Elp1* ^{Δ 20} allele), one *Elp1* allele with loxP sites flanking exon 20 (hypomorphic *Elp1*^{*Flox*} allele) and the human *TgFD9* transgene containing 9 copies of the complete *ELP1* gene into which we inserted the major IVS20+6T>C splice mutation^{36,38} (Supplementary Fig. S1). We first measured the expression levels of full-length *ELP1* transcript in each tissue and found a significant downregulation of full-length transcript in all five mouse neuronal tissues (Fig. 2A). In mouse tissues, the expression of FD full-length *ELP1* transcript compared to controls was 30.97% in DRG, 39.51% in TG, 44.56% in MED, 54.45% in Cortex, and 44.62% in SC. Next, we explored transcriptional ‘signatures’ representing the most significant transcriptional changes across tissues following *ELP1* reduction by performing DEG analyses and gating results on those with false discovery rate (FDR) less than 0.1 and fold changes (FCs) either greater than 1.2 (i.e. upregulated) or less than 0.8 (i.e. downregulated), compared to controls (see “Methods”). Using this approach, we observed 148 DEGs (FDR < 0.1) in DRG, 194 DEGs in TG, 65 DEGs in MED, 19 DEGs in SC and 59 DEGs in cortex (Fig. 2B, Supplementary Fig. S2A, Supplementary Table S1), demonstrating significantly higher dysregulation in the PNS tissues. As expected, *ELP1* was the most downregulated gene in all five tissues. The strongest increase in expression was observed with *Fev* (alias *Pet1*) in the DRG, TG, MED, and SC. *Fev* is a transcription factor known to play a crucial role in the differentiation and functional maturation of serotonergic neurons and displayed a 49-fold and 37-fold increase in expression in the DRG and TG respectively^{39–43} (Fig. 2B, Supplementary Table S1). In DRG and TG, we also observed upregulation of *Th* (1.66-fold in DRG and 2.14-fold in TG), which encodes a tyrosine hydroxylase and serves as a marker for dopaminergic neurons (Fig. 2B, Supplementary Table S1). Interestingly, the expression of the other Elongator subunits (*Elp2–6*) was not affected by the reduction of *ELP1* in any of the five mouse neuronal tissues (Supplementary Fig. S3).

We subsequently conducted functional enrichment analyses on the DEGs for each tissue using gene ontology (GO) to identify the pathways that were significantly enriched for DEGs in each FD neuronal tissue (see

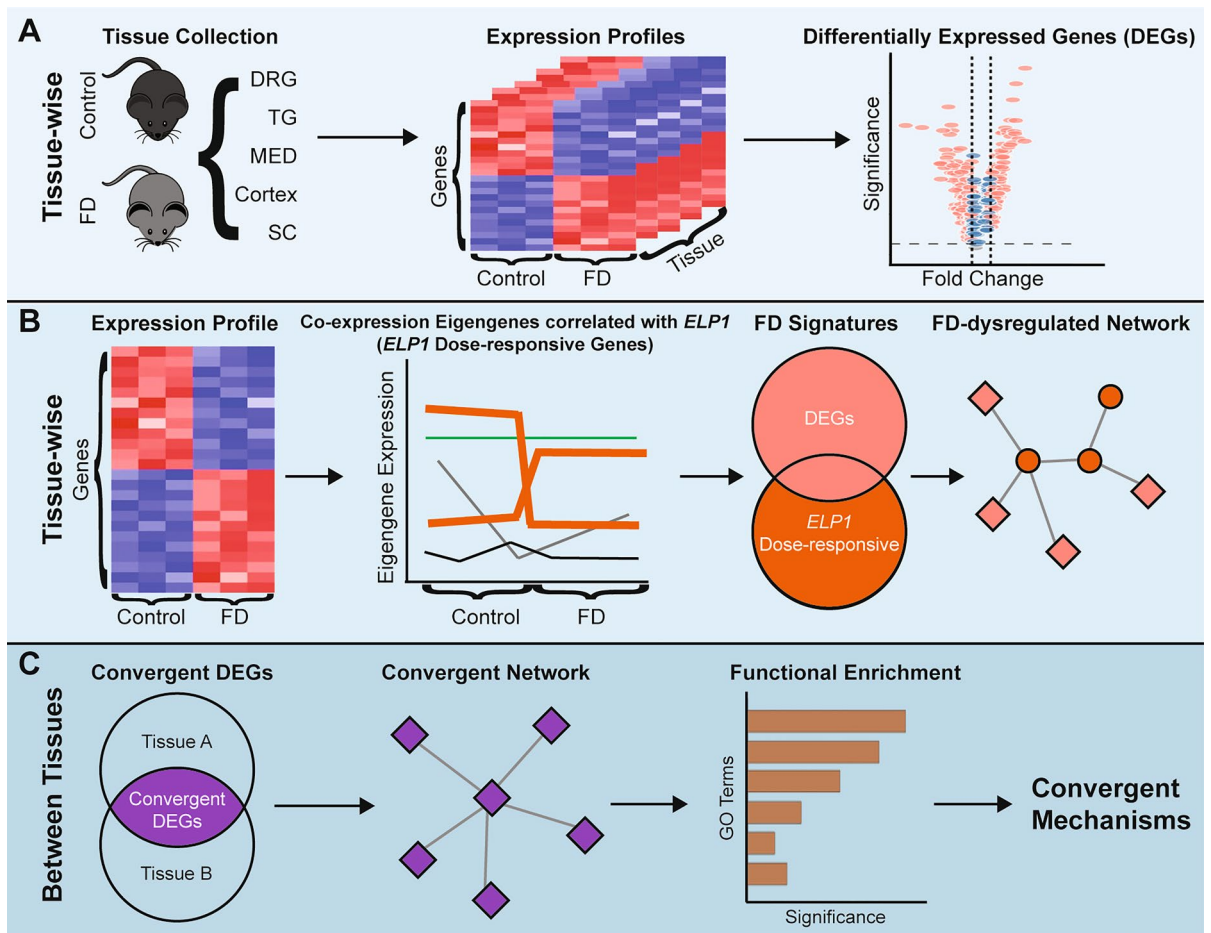


Figure 1. Experiment design and analysis workflow. (A) Tissue-specific DEG analyses to reveal the most dominant influence of *ELP1* reduction. (B) Assembly of FD gene signatures and the disrupted gene network by integrating DEGs and *ELP1* dose-responsive genes. (C) Identification of convergent disease mechanisms of FD across tissues using shared DEGs.

“Methods”, Supplementary Table S2). In DRG and TG, which exhibited the most pronounced gene expression dysregulation, we found DEGs were enriched in multiple GO terms associated with synaptic signaling and amine-related metabolic processes at FDR < 0.1 (Fig. 2C). Conversely, no significant enrichment was observed in CNS (Supplementary Fig. S2B).

The substantial number of observed DEGs, coupled with the significant enrichment of functional terms in the PNS, aligns with the observation of a drastic reduction (average ~65%) in full-length *ELP1* transcript within the PNS tissues. The dramatic *ELP1*-dependent gene dysregulation in the PNS is consistent with the significant neuronal loss observed in DRG from FD patients²⁵. The fact that an average 52% decrease in *ELP1* in the CNS does not result in dramatic gene dysregulation underscores different tissue-specific sensitivity to *ELP1* reduction.

Dose-responsive genes create a connection between the DEGs specific to each tissue and *ELP1* reduction

Although there were significant expression alterations (DEGs) between FD and control tissues, we did not observe a direct connection to *Elp1* in the mouse protein–protein interaction network (PPI). Therefore, we sought to identify *ELP1* dose-responsive genes, which are defined as genes that display co-expression and tight correlation with the level of full-length *ELP1* transcript³⁵. These genes are highly sensitive to *ELP1* dosage even though their expression does not significantly change between FD and control. To identify the *ELP1* dose-responsive genes, we adopted a two-step approach as previously described in Morini et al.³⁵. Initially, we identified co-expressed gene modules with eigengenes that correlate with full-length *ELP1* expression, followed by filtering for individual genes within these modules that display the strongest correlation (see “Methods”). As expected, each tissue had one co-expression module containing *Elp1* (Supplementary Table S3). Among 641 co-expression modules across five tissues, only seven modules (1.09%) in DRG, TG, and MED showed high correlation with the expression of full-length *ELP1* transcript (Supplementary Fig. S4A). In DRG, we identified 156 *ELP1* dose-responsive genes, while in TG and MED, we identified 137 and 514 such genes, respectively (Supplementary Fig. S4B–H, Supplementary Table S4).

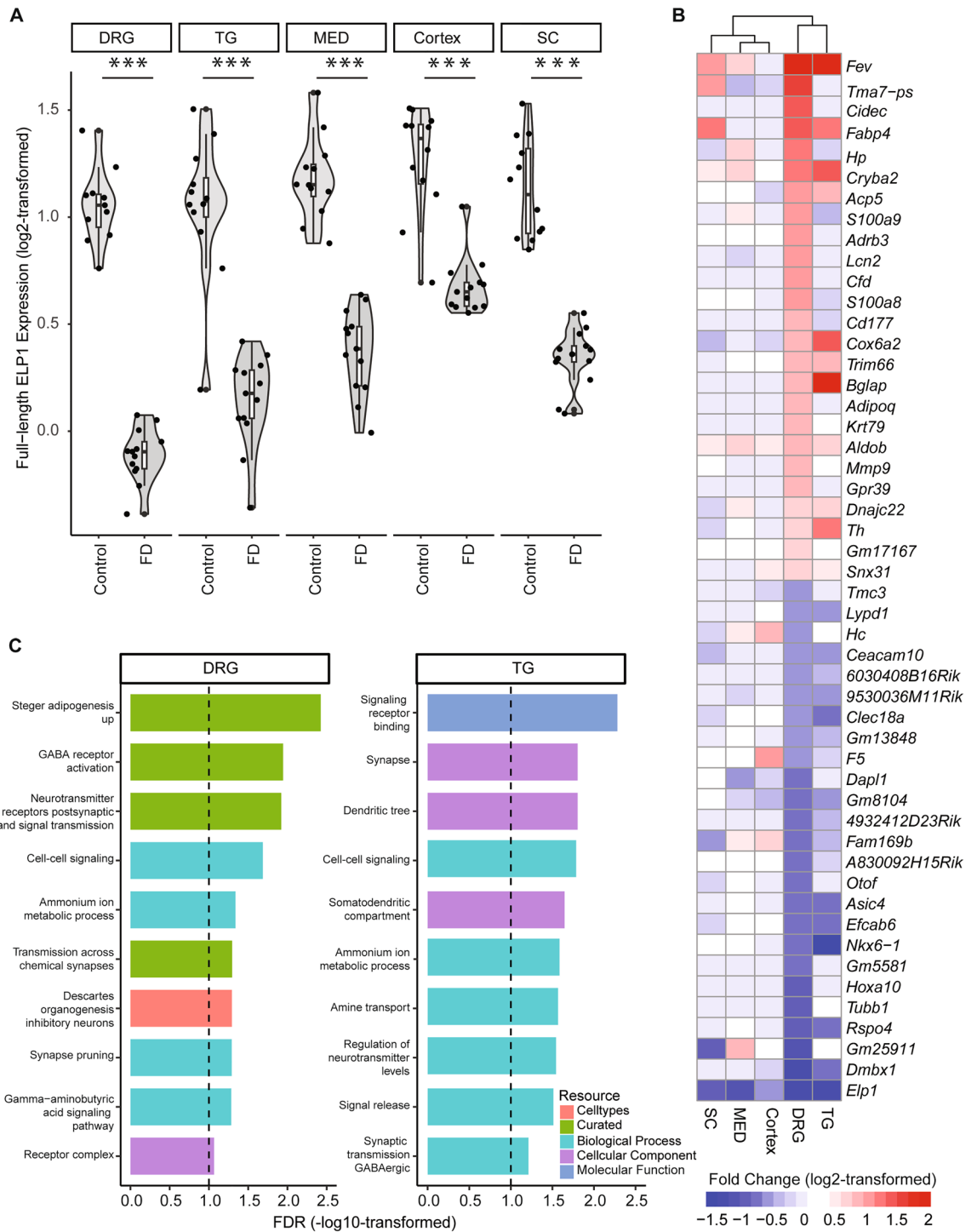


Figure 2. Tissue-specific DEGs and their functional enrichment. **(A)** The violin plot demonstrates the summed expression of full-length human ELP1 and mouse *Elp1* in counts per million (CPM, log₂-transformed) per tissue. The shape represents the distribution of expression values with individual points representing the actual CPM data points. The line in the middle of the box inside the violin distribution represents the median value with the upper and lower hinges of the box representing the first and third quartiles respectively. A *t*-test was used to calculate the *p*-value of the difference between FD and Control, followed by FDR correction. The ‘***’ indicates FDR < 0.001. **(B)** The heatmap represents the 25 most upregulated and downregulated genes between FD and Control across five tissues. Each row represents a gene, and each column represents a tissue. The red color domain represents upregulation between FD and Control while the blue color domain represents downregulation, where the expression changes are measured by log₂-transformed fold changes. The deeper the color, the stronger the fold changes. The range was set to [−1.5, 2]. Values beyond this range were clipped to either −1.5 or 2, whichever is closer. The rows are ordered, from top to bottom, by the greatest fold change across the five tissues. **(C)** Bar plot that represents the functional enrichment based on DEGs in DRG and TG, respectively. Note, only 10 significant terms (FDR < 0.1) are selected to display per tissue. The *x*-axis represents the enrichment significance in −log₁₀-transformed FDR while the *y*-axis represents the selected significant terms. The bar colors indicate the resources of GO. The vertical black dashed line represents an FDR of 0.1.

Next, we intersected DEGs and ELP1 dose-responsive genes to generate a set of tissue-specific FD signature genes that showed a strong correlation with ELP1 expression. Using the annotated mouse PPI data, we constructed gene networks to uncover the potentially disrupted molecular pathways in FD (see “Methods”) (Fig. 3A, Supplementary Fig. S5A). Interestingly in DRG, TG and MED we observed a significantly higher number of interactions among the FD signature genes compared to what would be expected by chance (PPI enrichment p -value $< 1.0E-12$, Fig. 3A, Supplementary Fig. S5A). In all three tissues, ELP1 was found to be connected to a network that encompassed at least 48% of the FD signature genes (DRG, 48.21% or 121/251; TG, 49.82% or 138/277, and MED 86.27% or 490/568, Supplementary Table S5). Notably, these networks highly relied on the inclusion of the *ELP1* dose-responsive genes (Fig. 3A, Supplementary Fig. S5A), as their exclusion resulted in an ELP1 network that contained less than 1% of the DEGs. For instance, in the DRG FD-dysregulated network, three *ELP1* dose-responsive genes, namely *Iars* (FDR = 0.041, fold change = 108%), *Asns* (FDR = 0.015, fold change = 110%), and *Aldh18a1* (FDR = 0.011, fold change = 111%), mediated the interactions between ELP1 and all network DEGs, except for *Hdhd3* and *Pxylp1* (Fig. 3A). *Iars* encodes isoleucyl-tRNA synthetase⁴⁴, *Asns* encodes asparagine synthetase⁴⁵, and *Aldh18a1* encodes pyroline-5-carboxylate synthetase⁴⁶, which are all associated with cellular amino acid metabolism. They establish connections between ELP1 and a series of solute carrier 7 (Slc7) family members, among which, Slc7a5 and Slc7a3, are responsible for neuronal amino acid transport across the cell membrane and are DEGs between FD and control^{47,48}.

The FD-dysregulated network in DRG showed several FD signature genes with five or more connections to their neighbors that serve as “hubs” within the network. It is noteworthy that 53.85% (21/39) of these hub genes were upregulated DEGs, while only 12.82% (5/39) of the hub genes were downregulated DEGs (Fig. 3B). To assess their relative contribution to the transcriptomic dysregulation observed in FD DRG, we ranked these hub genes based on their number of connections (Fig. 3B). The top five hubs that are DEGs in the network, *Rac2*, *Mmp9*, *Cxcl12*, *Hp*, and *Adipoq*, directly connect to 42.19% (27/64) of the network DEGs in DRG, as well as to each other. Further investigation into the molecular function of these genes and their role in maintaining neuronal health will provide valuable insights into the etiology of FD. We then examined the abundance of DEGs at different distances from ELP1 in the FD-dysregulated network of DRG, which provided insights into the influence of ELP1 reduction on the transcriptome. Interestingly, we found that 28.69% (72/251) of FD signature genes (and 26.35% DEGs) were located six to seven steps away from ELP1 in the DRG dysregulated network (Fig. 3C). In contrast, there were fewer FD signature genes (13.55%) within five steps of ELP1. This observation aligns with the placement of the top five hub genes within the network and suggests that the impact of reduced ELP1 levels may be amplified along the FD-dysregulated network in DRG.

The FD signature genes specific to TG showed significant enrichment in synaptic signaling, GABAergic synapse and neurotransmitter pathways (Supplementary Fig. S5A, Supplementary Table S6). Similar to DRG, the connection between ELP1 and the rest of the FD signature genes was mediated by an *ELP1* dose-responsive tRNA synthetase, *Cars*⁴⁹ (FDR = 0.0011, fold change = 113%, Supplementary Fig. S5A). Furthermore, like in DRG, the FD signature genes in TG are located far away from ELP1 (Supplementary Fig. S5B), and the majority (71.88%) of TG hub genes are significantly upregulated in FD compared to control samples (Supplementary Fig. S5C).

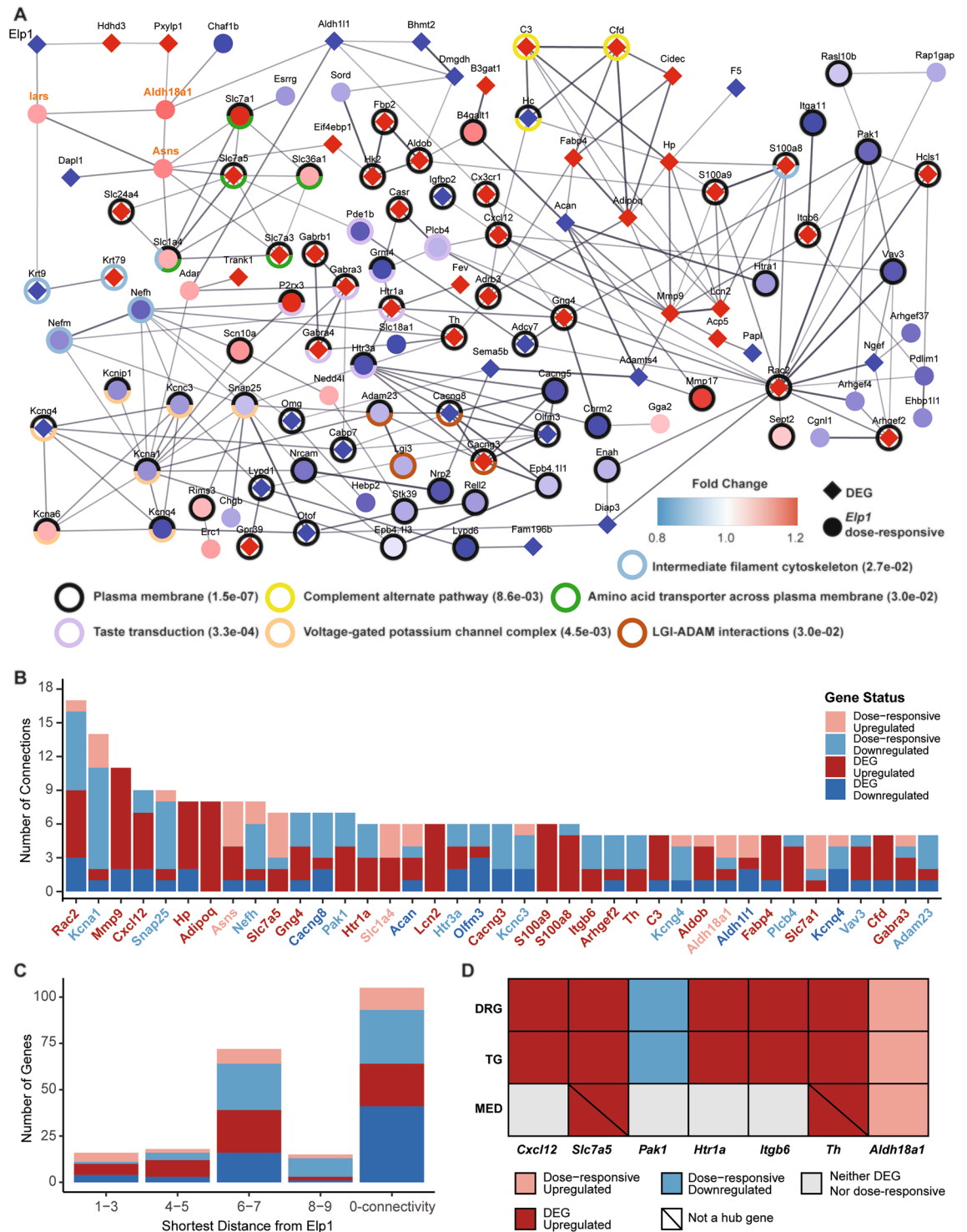
In MED, both the FD signature genes and FD-dysregulated gene network were distinct from those in the PNS tissues. Out of 568 FD signature genes specific to MED, 87.85% (499/568) were *ELP1* dose-responsive genes. The significant number of dose-responsive genes, coupled with the low count of DEGs, suggests a relatively mild impact of ELP1 reduction on the MED transcriptome. The FD signature genes were significantly enriched in the chromatin regulator term (Supplementary Fig. S6A, S6C, Supplementary Table S6), which was not observed in the FD signature genes of the PNS tissues. Additionally, these gene signatures were found to be closer to ELP1, with 63.38% (360/568) of MED signature genes located within four steps of ELP1 (Supplementary Fig. S6B).

Collectively, our findings indicate that ELP1 dose-responsive genes play a crucial role in mediating the connections between tissue-specific DEGs and ELP1. Furthermore, they nominate highly connected loci in the FD-regulatory gene network, shedding light on important contributors to the molecular etiology of FD.

Convergence of transcriptomic dysregulation in FD DRG and TG

We compared the hub genes across the three tissue-specific FD networks, and we discovered that seven hubs were shared between DRG and TG, while only one hub was shared by all three tissues (Fig. 3D, Supplementary Fig. S6D). To identify common and convergent molecular mechanisms underlying FD, we evaluated the extent of similarity between any two transcriptomes in relation to ELP1 reduction. From a differential expression perspective, we observed that DRG and TG shared 44 DEGs (~26%, $p = 4.55E-54$, hypergeometric test) enriched for synaptic signaling, dendrite tree development, and ammonium ion metabolic processes (Fig. 4B, Supplementary Table S7). In contrast, there were less than five overlapping DEGs between any two CNS tissues, although the number of overlaps was significantly different from what would be expected by chance (Fig. 4A). Among the three CNS tissues, only three DEGs, including *ELP1*, were shared (Supplementary Table S1).

The PNS convergent DEGs, when connected to ELP1 in both DRG- and TG-specific FD-dysregulated gene networks, exhibited a significantly similar distribution (Pearson correlation coefficient = 0.88, $p < 2.2E-16$) and were relatively distant from ELP1 (Fig. 4C). Additionally, the magnitude of dysregulation of these 44 PNS convergent DEGs was nearly identical, as indicated by a high Pearson correlation coefficient of 0.98 ($p < 2.2E-16$) for the fold change correlation between DRG and TG (Fig. 4D). Next, we compared the total level of transcriptomic disruption across tissues. We utilized the rank-rank hypergeometric overlap which evaluates the concordance of transcriptomic changes between any two tissues^{50,51}. The two PNS tissues exhibited the strongest concordance (odds ratio > 1 , Chi-squared test), whereas evidence of concordance among the CNS tissues was much weaker (refer to Supplementary Fig. S7, see “Methods”). Discordance became apparent when comparing a CNS tissue to a PNS tissue (Supplementary Fig. S7). We also found that 88.5% (46/52) of the co-expression modules in



DRG were preserved in TG (Fig. 4E). Taken together, these findings suggest convergent dysfunction in the two PNS tissues in FD.

PNS convergent DEGs show association with specific neuronal subtypes in FD

To gain a deeper understanding of how PNS convergent DEGs contribute to FD etiology, we hypothesized that the observed dysregulation might be driven by specific neuronal subtypes unique to the PNS. To investigate this, we analyzed publicly available single-cell RNA sequencing (scRNA-seq) data from wildtype mouse DRG^{42,52} and TG⁵³. By combining neuronal subtype markers provided in these studies with the novel markers identified through our analyses (Supplementary Fig. S8A–C, Supplementary Table S8, see “Methods”), we discovered significant overlaps with the DRG, TG, and PNS convergent DEGs (Fig. 5A). These sets of genes were enriched for specific neuronal subtype markers. Notably, we observed enrichment of markers for peptidergic nociceptors in

◀ **Figure 3.** Tissue-specific dysregulated gene network due to ELP1 reduction. **(A)** The dysregulated gene network in DRG. Each node is either a DEG indicated by a diamond shape or an ELP1 dose-responsive gene indicated by a round shape. The colors for the nodes reflect the fold changes in the genes between FD and Control. The red color domain represents upregulation between FD and Control while the blue color domain represents downregulation. The deeper the color, the stronger the fold changes. Each edge represents an interaction between the two connected genes, where only an interaction score of more than 0.4 (default) in String-DB is displayed. The thicker the edge, the higher the interaction score. Only the dysregulated genes with at least one interaction are displayed. The rings outside the nodes represent significant functional enrichment with $FDR < 0.1$ using all the dysregulated genes (i.e., DEGs and ELP1 dose-responsive genes). The names of three tRNA synthetases next to *Elp1* were marked in magenta. The associated functional enrichment terms with the ring colors are given, where the values in the brackets are the enrichment FDRs for the terms. **(B)** The bar plot demonstrates hub genes in DRG ranked by their number of connections to the neighbor genes in the network of panel (A). The *x*-axis represents the hub gene names, where each gene is colored according to its dysregulation direction and gene category. **(C)** The bar plot demonstrates the number of dysregulated genes in DRG at different distances to ELP1. The *x*-axis represents the distance of the shortest path to a gene. The genes in the “0-connectivity” distance category refer to those dysregulated genes not displayed in panel (A) because they don’t have any interaction score ≥ 0.4 . The *y*-axis represents the number of genes at each distance. **(D)** The table demonstrates the shared hub genes across DRG, TG, and MED. The rows represent the tissues while the columns represent the hub genes shared by at least two tissues. The colors of the grids reflect the genes’ categories and dysregulation directions.

DRG and TG, myelinated sensory neurons, and TH+ neurons in DRG, and c-fiber mechanoreceptors and cold nociceptors in TG (all FDRs < 0.07 , hypergeometric test). Furthermore, out of 44 PNS convergent DEGs, 15 were identified as neuronal subtype markers (Fig. 5B), with 11 of them being markers for peptidergic nociceptors and myelinated sensory neurons⁴². These findings suggest that these two neuronal subtypes might be particularly susceptible to ELP1 reduction in the PNS.

Collectively, our results provide novel insights into the dysregulation of peripheral nervous system gene expression in FD. Tissue-specific analyses revealed a greater impact of ELP1 reduction on PNS tissues compared to CNS tissues, as evidence by the number of DEGs. The FD-dysregulated gene networks showed upregulated hub genes that were significantly enriched in the PNS tissues. Cross-tissue comparisons further highlighted convergent mechanisms of disrupted synaptic signaling and amine-related metabolic processes in the PNS tissues, while such convergence was not observed across CNS tissues.

Discussion

FD is a progressive neurodegenerative disease that manifests in various debilitating symptoms including diminished pain and temperature perception, decreased or absent myotatic reflexes, proprioceptive ataxia, and retinal degeneration. Recent studies have provided compelling evidence linking the reduction of *Elp1* to sensory neuronal loss and diminished tissue innervation^{54–56}. However, the intricate molecular mechanisms connecting ELP1 reduction with the phenotypic manifestations of the disease remain largely unknown.

Using a humanized FD phenotypic mouse that recapitulates the same tissue-specific reduction of ELP1 observed in patients, we have conducted a comprehensive transcriptomic study to investigate the disrupted gene expression and pathways underlying FD etiology in disease-relevant neuronal tissues. We collected DRG and TG as representative PNS tissues, and cortex, MED, and SC as representative CNS tissues, from both control and FD-phenotypic mice. We found significant differences in the levels of full-length *ELP1* transcripts between PNS and CNS. The PNS tissues, DRG and TG, exhibited lower levels of full-length *ELP1* transcripts (~35% of the control level) when compared to the three CNS tissues, MED, cortex, and SC (~48% of the control level).

To gain deeper insights into the molecular networks and pathways involved in FD, we assembled a set of FD signature genes by combining tissue-specific DEGs that represented the most prominent transcriptional alterations, and ELP1 dose-responsive genes that exhibited moderate expression changes but they closely correlated with ELP1 levels. The FD signature genes formed interconnected gene networks providing a comprehensive view of how ELP1 reduction impacts the expression of many genes. This study shows that merely using DEGs is not sufficient to build a meaningful PPI network. Adding dose–response genes interconnects the robust signals from DEGs and creates a more interconnected and expansive network. FD is a recessive disease but, unlike most recessive diseases, it does not result from complete loss of a protein but is caused by tissue-specific reduction of ELP1^{57,58}. It is reasonable to think that the reduction of ELP1, instead of its complete depletion, might cause moderate transcriptomic changes (e.g. *ELP1* dose-responsive genes) in its immediate downstream genes. These moderate responders could then synergistically lead to more dramatic expression alterations (DEGs) deeper in the molecular network. We indeed observed such patterns in both DRG and TG FD-dysregulated networks.

In the DRG, for instance, the connection of *Elp1* with the other DEGs is dependent on the inclusion of the three dose-responsive genes *lars*, *Aldh18a1* and *Asns* (Fig. 3A). These three genes encode synthase proteins. It is well known that the cellular concentrations of tRNA synthase must be precisely regulated and overproduction of them leads to various disorders including neurodegeneration^{23,59,60}. In addition, we observed significant upregulation of amino acid transporter genes *Slc7a5* (alias *Lat1*) and *Slc7a3* (alias *Cat3*). Both tRNA synthesis and amino acid transport are the immediate upstream biological steps of tRNA wobble modification, one of the well-studied functions of *ELP1*^{13,15,23,59,61}. Interestingly, the expression of the other Elongator subunits (*Elp2–6*) was not affected by the reduction of ELP1. This suggests that the expression of each subunit might be independently regulated, and they may not be linked by negative feedback regulation. However, it is important to note

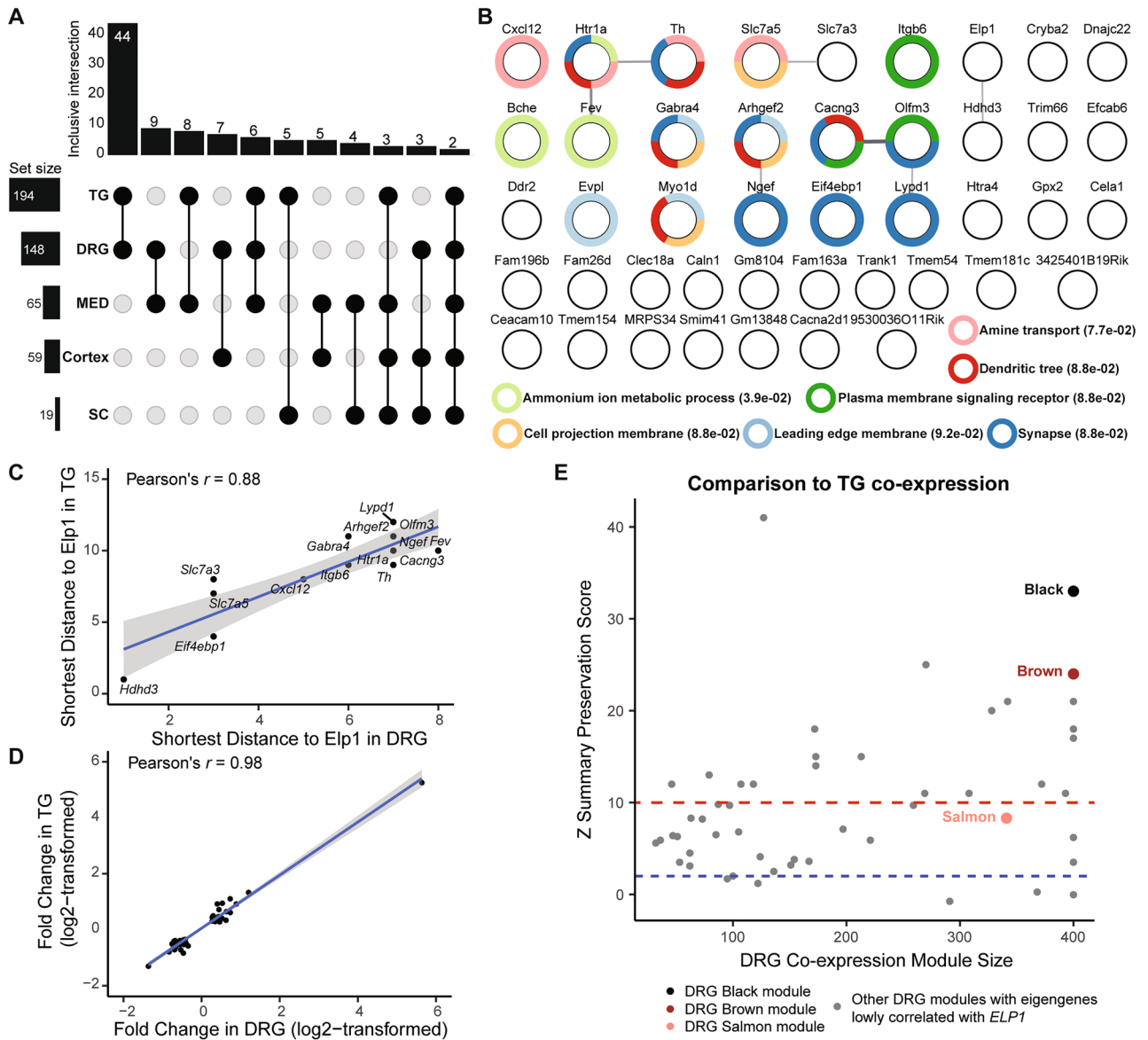


Figure 4. The convergence of transcriptomic dysregulation in the PNS tissues. **(A)** The UPSET plot demonstrates the DEGs overlaps between two out of the five tissues. The x-axis of the bar plot represents overlap comparisons while the y-axis of it represents the number of genes. **(B)** The gene network of PNS convergent DEGs. Each node represents a PNS convergent DEG indicated by a round shape. Each edge represents a potential interaction between the two connected genes, where only an interaction score of more than 0.4 (default) in String-DB is displayed. The thicker edge, the higher the interaction score. The rings outside the nodes represent significant functional enrichment with $FDR < 0.1$ of all the PNS convergent DEGs. The associated functional enrichment terms with the ring colors are given, where the values in the brackets are the enrichment FDRs for the terms. **(C)** The scatter plot demonstrates the shortest distances of PNS convergent DEGs from ELP1 in the DRG dysregulated network (x-axis) and the TG dysregulated network (y-axis), respectively. Each dot represents a PNS convergent DEG with non-zero connectivity in both networks. The blue line represents the best-fitted linear regression line while the grey zone around the line represents the 95% confidence intervals. **(D)** The scatter plot demonstrates the log₂-transformed fold change of PNS convergent DEGs in DRG (x-axis) and TG (y-axis), respectively. Each dot represents a PNS convergent DEG. The blue line represents the best-fitted linear regression line while the grey zone around the line represents the 95% confidence intervals. **(E)** The scatter plot demonstrates the DRG co-expression modules' sizes (x-axis) and their similarity to the TG co-expression modules, measured by Z summary preservation scores (y-axis). The score indicates the degree of relatedness of each module to other modules in other co-expression networks. The dots represent the co-expression modules identified in DRG. The three modules whose eigengene highly correlated with the full-length ELP1 expression, namely black, brown, and salmon, are highlighted in their corresponding colors. The blue dashed line indicates a module preservation score of 2 below which the preservation is not considered strong, while the red dashed line represents a module preservation score of 10 above which the preservation is considered very strong.

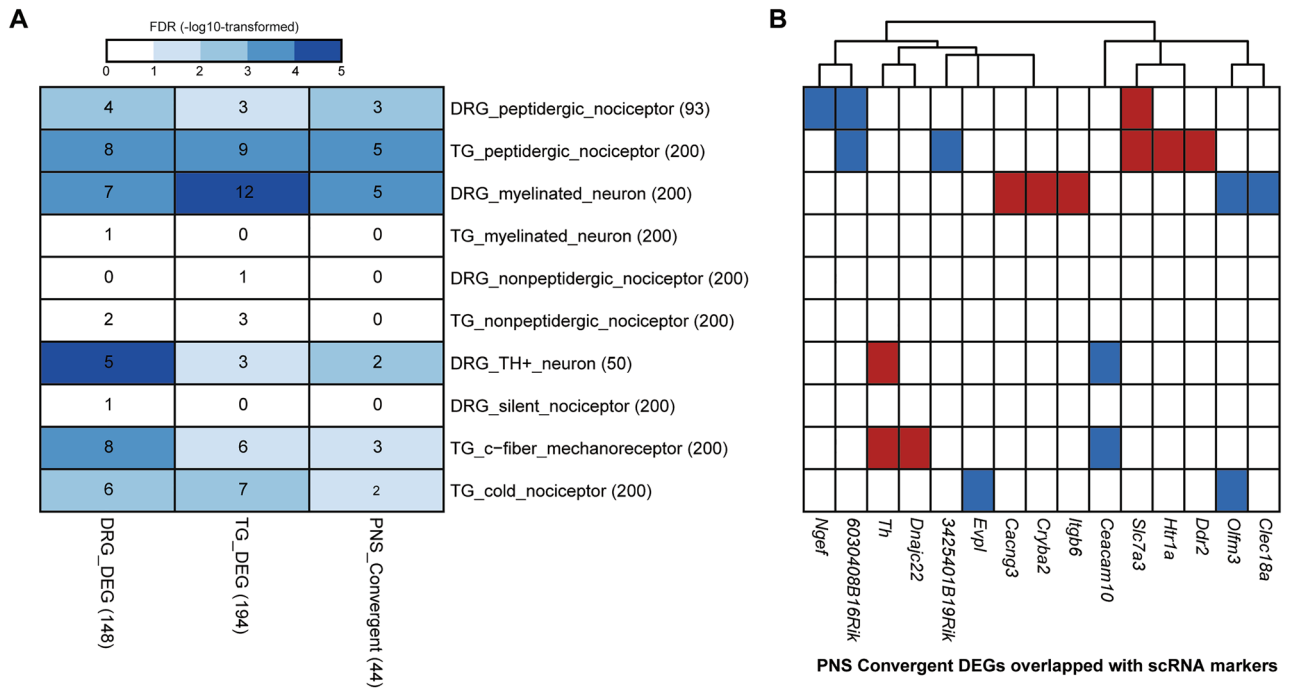


Figure 5. The potential transcriptomic dysregulation at neuronal subtype levels in the PNS tissues. **(A)** The heatmap demonstrates the overlap between DEGs identified from this study (columns) and the neuronal subtype markers identified from publicly available scRNA datasets for mouse DRG and TG. The numbers in the brackets after the row or column names indicate the number of genes in each category. The numbers in the grids indicate the number of gene overlaps between the two categories. The grid colors reflect the significance of overlap according to the hypergeometric test followed by FDR correction, in the $-\log_{10}$ -transformed scale. The deeper the color, the more significant the overlap. The grids in white mean no significant overlap where $FDR > 0.1$. **(B)** The overlaps between the PNS convergent DEGs (columns) and the neuronal subtype markers identified from publicly available scRNA datasets for mouse DRG and TG (rows, the same as panel **(A)**). The colors of the grids reflect the genes' dysregulation directions between FD and Control, where red is for upregulation while blue is for downregulation.

that the functional integrity of Elongator is compromised in the absence of any of its subunits^{13,62}. Therefore, the observed dysregulation is likely a result of the compromised function of the entire Elongator complex. We acknowledge that these findings are based on the expression profiles identified from an FD-phenotypic mouse model and rely on the annotated mouse PPI network. Further evaluation is needed to determine the extent to which these findings can be translated to FD patients. Transcriptome-wide, we observed striking similarities in the response to ELP1 reduction between DRG and TG. The PNS convergent DEGs in this study were enriched for synaptic signaling and amine transport. This PNS enrichment aligns with the functional enrichment patterns observed in DEGs specific to each tissue. Further exploration of these convergent and tissue-specific DEGs may provide valuable insights into the underlying mechanisms of FD.

Finally, to determine if the observed dysregulation was specific to unique neuronal subtypes in the PNS, we combined the markers identified through our analyses with mouse DRG and TG neuronal subtype markers from publicly available single-cell RNA sequencing (scRNA-seq) data^{42,52,53}. Remarkably, we found significant overlaps between the PNS convergent DEGs and the single-cell markers associated with peptidergic nociceptors and myelinated sensory neurons supporting the hypothesis that certain neuronal subtypes are more susceptible to ELP1 reduction.

Overall, our study provided a comprehensive analysis of the disrupted transcriptomic dynamics in FD from both tissue-specific and cross-tissue perspectives. By examining gene expression patterns, we identified several gene sets that may contribute to the disease manifestations. The FD signature genes in the PNS tissues were found to be enriched in amine-related metabolic processes, which in turn influenced synaptic signaling. Our findings suggest the peptidergic nociceptors and myelinated sensory neurons in the PNS are particularly affected in FD, as evidenced by significant alterations in the expression of their marker genes upon ELP1 reduction. Our study not only provides valuable insights into the intricate molecular mechanisms underlying FD but also has broader implications for other neurological disorders associated with Elongator dysfunction.

Methods

Animals

The generation of the *TgFD9* mouse line carrying the human *ELP1* transgene with the NM_003640.5:c.2204+6T>C mutation can be found in Hims et al.³⁸. Descriptions of the original targeting vector used to generate the *Elp1^{flox}* allele and the strategy to generate the *Elp1^{Δ20}* allele have been previously published^{63,64}.

To generate the experimental *TgFD9*; *Elp1^{Δ20/flox}* mouse, we crossed the *TgFD9* transgenic mouse heterozygous for the *Elp1^{flox}* allele (*TgFD9^{+/-}*; *Elp1^{flox/+}*) with each other. Pups were genotyped to identify those homozygotes for both the *TgFD9* transgene and the *Elp1^{flox}* allele (F1: *TgFD9^{+/+}*; *Elp1^{flox/flox}*). These animals were then crossed with the mouse line heterozygous for the *Elp1^{Δ20}* allele (*Elp1^{Δ20/+}*) to generate the FD mouse *TgFD9*; *Elp1^{Δ20/flox}* (F2). Controls are littermates of the FD mice that carry the transgene but are phenotypically normal because they express the endogenous *Elp1* gene (*TgFD9^{+/-}*; *Elp1^{+/+}*, *TgFD9^{+/-}*; *Elp1^{flox/+}* or *TgFD9^{+/-}*; *Elp1^{Δ20/+}*). Both sexes were included in this study. The mice were housed in the animal facility at Massachusetts General Hospital (Boston, MA, USA), provided with access to food and water ad libitum, and maintained on a 12-h light/dark cycle.

For routine genotyping of progeny, genomic DNA was prepared from tail biopsies, and PCR was carried out using the following primers—forward, 5'-TGATTGACACAGACTCTGGCCA-3'; reverse, 5'-CTTTCCTACTCTGA AATTACAGGAAG-3'—to discriminate the *Elp1* alleles and the primers—forward 5'-GCCATTGTACTGTTT GCGACT-3'; reverse, 5'-TGAGTGTACGATTCTTTCTGC-3'—to detect the *TgFD9* transgene.

All experimental protocols were approved by the Institutional Animal Care and Use Committee of the Massachusetts General Hospital and were in accordance with ARRIVE (<https://arriveguidelines.org/>) and NIH guidelines.

Tissue-specific RNA-seq

RNA was extracted from DRG, trigeminal ganglion, cortex, medulla, and spinal cord collected from 12 control (6 males and 6 females) and 13 FD (4 males and 9 females) 3-month-old mice. Using the QIAzol Reagent, following the manufacturer's instructions. RNA-seq libraries were prepared using the Tru-Seq Stranded mRNA library Prep Kit (Illumina, 20020594) using 100 ng of total RNA as input. Final library concentration was quantified using size distribution by the Agilent 2200 Tape Station and/or qPCR using the Library Quantification Kit (KK4854, Kapa Biosystems). Equimolar amounts of each library were pooled prior to multiplex sequencing. Libraries were 50 basepair paired end sequenced on the Illumina HiSeq 2500 across multiple lanes. The HiSeq Sequencing Control Software was used for real-time image analysis and base calling before CASAVA (version 1.8) was used for FastQ generation.

RNA-seq pre-processing

A custom transcriptome reference was generated by adding the human *ELP1* gene (ENSG00000070061) Ensemble Human transcriptome reference GRCh37.75 to the Ensembl Mouse Transcriptome GRCm38.83 as an independent chromosome. RNA-seq reads were mapped to this synthesized transcriptome reference by STAR v2.5.22b allowing only uniquely mapped reads with 5% mismatch⁶⁵. Illumina TruSeq reads were trimmed using Trimmomatic (v0.36) with minimal length set to 105 and other default parameters⁶⁶.

Differential gene expression analysis

Gene counts were performed via HTSeq-counts⁶⁷ (version 0.11.2) with '-s reverse' option to be compatible with the Illumina TruSeq library. Genes were further filtered so that only genes whose median expression was no less than 0.1 counts-per-million in at least one genotype were kept for analysis. Raw gene counts were then normalized using sample-wise size factors estimated by the Bioconductor package DESeq2⁶⁸ (v1.34.0). To get the most robust DEGs between the two genotypes of interest (FD and control), surrogate variables unrelated to genotype were first estimated from the normalized counts via the Bioconductor package SVA⁶⁹ (v3.42.0) and then built into a generalized linear model (GLM) together with genotype via DESeq2. Data from both males and females were combined for this analysis. We performed a correlation analysis on several parameters including sex with principal components and surrogate variables. Sex was corrected by surrogate variable analysis and did not correlate with any principal components. Since the phenotypes in FD patients do not exhibit sex differences^{1,25}, in this study we aimed at identifying the common disease mechanism regardless of sex.

Concordance of FD transcriptomic dynamics between tissues

To assess the similarity of the transcriptomic response we compared the expression changes between FD and Control across any two tissues using the Rank-Rank Hypergeometric Overlap test via the RRHO2 Bioconductor package^{50,51}. The significance of overlap was calculated in log-transformed odds ratio from the Chi-squared test.

Gene networks according to PPI

These networks were built to include the query gene sets using the "stringApp"⁷⁰ (version 2.0.1) in Cytoscape⁷¹ (version 3.9.1). For a tissue-specific FD-dysregulated gene network, the query set consisted of tissue-specific DEGs and *ELP1* dose-responsive genes. For the PNS convergent network, the query set consisted of shared DEGs between DRG and TG. To construct each network, the "STRING: protein query" mode was used, with species set as "*Mus musculus*", confidence (score) cutoff set as 0.4 and maximum additional interactor set as 0.

Shortest distance from Elp1

The "Edge Table" from the stringApp network construction was exported. A customized R script was used to convert the pair-wised interactions in the "Edge Table" to an R list object, where the list names represented the

nodes (i.e., genes) in the network while the list elements were vectors representing genes connected to each node. Then the shortest distance was calculated via the “shortest_paths” function from an opensource R package “igraph” (version 1.3.5, <https://github.com/igraph/igraph>).

GO analysis

In each analysis, the query gene set was searched against a background gene list consisting of either expressed genes from the same tissue or non-redundant union of expressed genes from multiple tissues where the query set was built from. For functional enrichment of tissue-specific DEGs, the resources of GO were from the Gene Set Enrichment Analysis website⁷² (<https://www.gsea-msigdb.org/>, v. MS1). For functional enrichment of FD signature genes or PNS convergent DEGs that were used to build interaction networks, the “Functional enrichment” function from the stringApp in Cytoscape was used, with the appropriate background expressed genes as reference. For any two significant functional terms, an overlap score was calculated to reflect their semantic similarity. An overlap score cutoff of either 0.1 or 0.2 was applied on the raw result to remove redundancy in the results.

For all the functional enrichment analyses in this study, complete lists of the results were provided in the supplementary tables.

Co-expression module analysis

Once generalized linear models for differential gene expression were established, the effects from surrogate variables were regressed out from the normalized gene counts to create a cleaned matrix whose variance was mainly due to the genotype difference. Then the R package WGCNA⁷³ (version 1.71) was implemented upon this cleaned matrix of each tissue, identifying genes co-expressed together and grouping them into modules. To achieve the best performance, the soft-thresholding power was heuristically selected for each tissue (cortex power = 5, dorsal root ganglion power = 6, medulla power = 5, spinal cord power = 6, trigeminal ganglion power = 7) at the beginning of the WGCNA approach. A signed network was used, and minimal module size was set to 30 and the raw modules were merged with a dis-similarity cut-off of 0.25.

Correlation between co-expression modules’ eigengenes and the full-length *ELP1* expression

The full-length *ELP1* transcript expression was measured as the expression sum of exon 20 (human) and exon 26 (mouse), in the unit of counts per million (CPM). The values across all samples from the same tissue were correlated with each eigengene representing the identified co-expression modules using Pearson correlation. *ELP1* dose-responsive genes were defined as the genes meeting both of the following criteria: (1) the Pearson correlation between their co-expression module eigengene and the full-length *ELP1* had a coefficient no less than 0.8; and (2) the absolute value of the Pearson correlation coefficient between their normalized expression and the module eigengene had a coefficient no less than 0.8.

Analysis of publicly available scRNA-seq data

For DRG scRNA-seq, the processed data was downloaded from GEO (GSE59739). Cells with the top and bottom 2.5% of the number of RNA features were filtered out. The normalized counts were what the authors provided^{42,52,53}. Dimensionality reduction was first done via multiple correspondence analysis (MCA) using the CelliD package⁷⁴ (version 1.6.0), followed by uniform manifold approximation and projection (UMAP) using the Seurat package⁷⁵ (version 4.2.1). Unsupervised clustering was done in the UMAP space using 20-nearest neighbor graph construction with a resolution of 0.2. For each unsupervised cluster, its gene signatures were defined as the top 200 nearest genes to the cluster (i.e., cells) center in the MCA space. The cell-type markers provided by the authors were then compared with the unsupervised cluster signatures. If the overlap was significant under the hypergeometric test, the unsupervised cluster would be marked as the cell-type provided by the authors and the cell-type markers would be replaced by the unsupervised cluster signatures. If the cell-type provided by the authors was found to have no significant overlaps with the markers from the unsupervised clusters, the authors’ cell-types and markers were retained in the final marker list.

For TG scRNA-seq, the raw counts data were downloaded from GEO (GSE197289). Cells with top and bottom 2.5% of the number of RNA features were filtered out. Normalization was done using SCTransform package⁷⁶ (version 0.3.5), with variance stabilization flavor set to “v2”. Like the DRG processing, the dimension reduction was done by MCA followed by UMAP. The UMAP visual separation already agreed with the cell types provided by the authors. The signature of each cell type was called by the top 200 nearest genes to the cell-type center in the MCA space.

Statistical analysis

Wald test was used to estimate the significance of DEGs from the DESeq2 models. Within each tissue, genes with false discovery rate (FDR) < 0.1 and a fold change cut-off was applied (more than 120% for upregulated or less than 80% for downregulated genes) and these genes were then considered as significant. Fisher’s exact test was used for GO analysis where a significant enrichment was defined as FDR < 0.1. A significant correlation throughout this study was defined as Pearson correlation coefficient ≥ 0.8 . For overlap significance, hypergeometric test was used and the *p*-value < 0.05 (or FDR < 0.1 when multiple test correction was applicable) was considered as significant. The four values used in the hypergeometric test were the size of gene list A, gene list B, their overlaps, and their non-redundant background genes (e.g., all expressed genes in the transcriptome where list A and B derived from).

Data availability

RNA-seq raw and processed data used in this study is available at GSE230867.

Received: 31 October 2023; Accepted: 31 December 2023

Published online: 04 January 2024

References

- Norcliffe-Kaufmann, L., Slaugenhaupt, S. A. & Kaufmann, H. Familial dysautonomia: History, genotype, phenotype and translational research. *Prog. Neurobiol.* **152**, 131–148. <https://doi.org/10.1016/j.pneurobio.2016.06.003> (2017).
- Cuajungco, M. P. *et al.* Tissue-specific reduction in splicing efficiency of IKBKAP due to the major mutation associated with familial dysautonomia. *Am. J. Hum. Genet.* **72**, 749–758. <https://doi.org/10.1086/368263> (2003).
- Krogan, N. J. & Greenblatt, J. F. Characterization of a six-subunit holo-elongator complex required for the regulated expression of a group of genes in *Saccharomyces cerevisiae*. *Mol. Cell. Biol.* **21**, 8203–8212. <https://doi.org/10.1128/mcb.21.23.8203-8212.2001> (2001).
- Hawkes, N. A. *et al.* Purification and characterization of the human elongator complex. *J. Biol. Chem.* **277**, 3047–3052. <https://doi.org/10.1074/jbc.M110445200> (2002).
- Li, F., Lu, J., Han, Q., Zhang, G. & Huang, B. The Elp3 subunit of human elongator complex is functionally similar to its counterpart in yeast. *Mol. Genet. Genom.* **273**, 264–272. <https://doi.org/10.1007/s00438-005-1120-2> (2005).
- Chen, Z. *et al.* Mutations in ABO1/ELO2, a subunit of holo-Elongator, increase abscisic acid sensitivity and drought tolerance in *Arabidopsis thaliana*. *Mol. Cell. Biol.* **26**, 6902–6912. <https://doi.org/10.1128/mcb.00433-06> (2006).
- Chen, Y. T. *et al.* Loss of mouse Ikbkap, a subunit of elongator, leads to transcriptional deficits and embryonic lethality that can be rescued by human IKBKAP. *Mol. Cell. Biol.* **29**, 736–744. <https://doi.org/10.1128/mcb.01313-08> (2009).
- Kojic, M. & Wainwright, B. The many faces of elongator in neurodevelopment and disease. *Front. Mol. Neurosci.* **9**, 115. <https://doi.org/10.3389/fnmol.2016.00115> (2016).
- Rahl, P. B., Chen, C. Z. & Collins, R. N. Elp1p, the yeast homolog of the FD disease syndrome protein, negatively regulates exocytosis independently of transcriptional elongation. *Mol. Cell* **17**, 841–853 (2005).
- Close, P. *et al.* Transcription impairment and cell migration defects in elongator-depleted cells: Implication for familial dysautonomia. *Mol. Cell* **22**, 521–531 (2006).
- Tourtellotte, W. G. Axon transport and neuropathy: Relevant perspectives on the etiopathogenesis of familial dysautonomia. *Am. J. Pathol.* **186**, 489–499. <https://doi.org/10.1016/j.ajpath.2015.10.022> (2016).
- Naftelberg, S. *et al.* Phosphatidylserine ameliorates neurodegenerative symptoms and enhances axonal transport in a mouse model of familial dysautonomia. *PLoS Genet.* **12**, e1006486. <https://doi.org/10.1371/journal.pgen.1006486> (2016).
- Huang, B., Johansson, M. J. & Byström, A. S. An early step in wobble uridine tRNA modification requires the Elongator complex. *RNA* **11**, 424–436. <https://doi.org/10.1261/rna.7247705> (2005).
- Esberg, A., Huang, B., Johansson, M. J. & Byström, A. S. Elevated levels of two tRNA species bypass the requirement for elongator complex in transcription and exocytosis. *Mol. Cell* **24**, 139–148. <https://doi.org/10.1016/j.molcel.2006.07.031> (2006).
- Bauer, F. & Hermand, D. A coordinated codon-dependent regulation of translation by Elongator. *Cell Cycle* **11**, 4524–4529. <https://doi.org/10.4161/cc.22689> (2012).
- Chen, W. T. *et al.* Elp1 facilitates RAD51-mediated homologous recombination repair via translational regulation. *J. Biomed. Sci.* **28**, 81. <https://doi.org/10.1186/s12929-021-00773-z> (2021).
- Creppe, C. *et al.* Elongator controls the migration and differentiation of cortical neurons through acetylation of α -tubulin. *Cell* **136**, 551–564 (2009).
- Xu, Y. *et al.* Elongator promotes the migration and invasion of hepatocellular carcinoma cell by the phosphorylation of AKT. *Int. J. Biol. Sci.* **14**, 518 (2018).
- Kim, J. H., Lane, W. S. & Reinberg, D. Human Elongator facilitates RNA polymerase II transcription through chromatin. *Proc. Natl. Acad. Sci. USA* **99**, 1241–1246. <https://doi.org/10.1073/pnas.251672198> (2002).
- Wittschieben, B. O. *et al.* A novel histone acetyltransferase is an integral subunit of elongating RNA polymerase II holoenzyme. *Mol. Cell* **4**, 123–128. [https://doi.org/10.1016/s1097-2765\(00\)80194-x](https://doi.org/10.1016/s1097-2765(00)80194-x) (1999).
- Dauden, M. I. *et al.* Molecular basis of tRNA recognition by the Elongator complex. *Sci. Adv.* **5**, eaaw2326. <https://doi.org/10.1126/sciadv.aaw2326> (2019).
- Lin, T. Y. *et al.* The Elongator subunit Elp3 is a non-canonical tRNA acetyltransferase. *Nat. Commun.* **10**, 625. <https://doi.org/10.1038/s41467-019-08579-2> (2019).
- Goffena, J. *et al.* Elongator and codon bias regulate protein levels in mammalian peripheral neurons. *Nat. Commun.* **9**, 889. <https://doi.org/10.1038/s41467-018-03221-z> (2018).
- Norcliffe-Kaufmann, L. & Kaufmann, H. Familial dysautonomia (Riley-Day syndrome): When baroreceptor feedback fails. *Auton. Neurosci.* **172**, 26–30. <https://doi.org/10.1016/j.autneu.2012.10.012> (2012).
- Pearson, J., Pytel, B. A., Grover-Johnson, N., Axelrod, F. & Dancis, J. Quantitative studies of dorsal root ganglia and neuropathologic observations on spinal cords in familial dysautonomia. *J. Neurol. Sci.* **35**, 77–92. [https://doi.org/10.1016/0022-510x\(78\)90103-x](https://doi.org/10.1016/0022-510x(78)90103-x) (1978).
- Axelrod, F. B., Nachtigal, R. & Dancis, J. Familial dysautonomia: Diagnosis, pathogenesis and management. *Adv. Pediatr.* **21**, 75–96 (1974).
- Morini, E. *et al.* ELP1 splicing correction reverses proprioceptive sensory loss in familial dysautonomia. *Am. J. Hum. Genet.* **104**, 638–650. <https://doi.org/10.1016/j.ajhg.2019.02.009> (2019).
- Cascella, M. *et al.* Pathophysiology of nociception and rare genetic disorders with increased pain threshold or pain insensitivity. *Pathophysiology* **29**, 435–452 (2022).
- Axelrod, F. B. *et al.* Progressive sensory loss in familial dysautonomia. *Pediatrics* **67**, 517–522 (1981).
- González-Duarte, A., Cotrina-Vidal, M., Kaufmann, H. & Norcliffe-Kaufmann, L. Familial dysautonomia. *Clin. Auton. Res.* **33**, 269–280 (2023).
- Morini, E. *et al.* Development of an oral treatment that rescues gait ataxia and retinal degeneration in a phenotypic mouse model of familial dysautonomia. *Am. J. Hum. Genet.* **110**, 531–547 (2023).
- Abashidze, A., Gold, V., Anavi, Y., Greenspan, H. & Weil, M. Involvement of IKAP in peripheral target innervation and in specific JNK and NGF signaling in developing PNS neurons. *PLoS One* **9**, e113428. <https://doi.org/10.1371/journal.pone.0113428> (2014).
- George, L. *et al.* Familial dysautonomia model reveals Ikbkap deletion causes apoptosis of Pax3+ progenitors and peripheral neurons. *Proc. Natl. Acad. Sci. USA* **110**, 18698–18703. <https://doi.org/10.1073/pnas.1308596110> (2013).
- Lee, G. *et al.* Modelling pathogenesis and treatment of familial dysautonomia using patient-specific iPSCs. *Nature* **461**, 402–406. <https://doi.org/10.1038/nature08320> (2009).
- Morini, E. *et al.* Developmental regulation of neuronal gene expression by Elongator complex protein 1 dosage. *J. Genet. Genom.* **49**, 654–665. <https://doi.org/10.1016/j.jgg.2021.11.011> (2022).
- Morini, E. *et al.* Sensory and autonomic deficits in a new humanized mouse model of familial dysautonomia. *Hum. Mol. Genet.* **25**, 1116–1128. <https://doi.org/10.1093/hmg/ddv634> (2016).
- Chekuri, A. *et al.* Selective retinal ganglion cell loss and optic neuropathy in a humanized mouse model of familial dysautonomia. *Hum. Mol. Genet.* **31**, 1776–1787. <https://doi.org/10.1093/hmg/ddab359> (2022).

38. Hims, M. M. *et al.* A humanized IKBKAP transgenic mouse models a tissue-specific human splicing defect. *Genomics* **90**, 389–396 (2007).
39. Okaty, B. W., Commons, K. G. & Dymecki, S. M. Embracing diversity in the 5-HT neuronal system. *Nat. Rev. Neurosci.* **20**, 397–424. <https://doi.org/10.1038/s41583-019-0151-3> (2019).
40. Fozard, J. R. Neuronal 5-HT receptors in the periphery. *Neuropharmacology* **23**, 1473–1486. [https://doi.org/10.1016/0028-3908\(84\)90091-1](https://doi.org/10.1016/0028-3908(84)90091-1) (1984).
41. Maurer, P. *et al.* FEV acts as a transcriptional repressor through its DNA-binding ETS domain and alanine-rich domain. *Oncogene* **22**, 3319–3329. <https://doi.org/10.1038/sj.onc.1206572> (2003).
42. Tavares-Ferreira, D. *et al.* Spatial transcriptomics of dorsal root ganglia identifies molecular signatures of human nociceptors. *Sci. Transl. Med.* **14**, 8186 (2022).
43. Wyler, S. C. *et al.* Pet-1 switches transcriptional targets postnatally to regulate maturation of serotonin neuron excitability. *J. Neurosci.* **36**, 1758–1774. <https://doi.org/10.1523/jneurosci.3798-15.2016> (2016).
44. Nichols, R. C. *et al.* Assignment of two human autoantigen genes-isoleucyl-tRNA synthetase locates to 9q21 and lysyl-tRNA synthetase locates to 16q23-q24. *Genomics* **36**, 210–213. <https://doi.org/10.1006/geno.1996.0449> (1996).
45. Heng, H. H., Shi, X. M., Scherer, S. W., Andrusis, I. L. & Tsui, L. C. Refined localization of the asparagine synthetase gene (ASNS) to chromosome 7, region q21.3, and characterization of the somatic cell hybrid line 4AF/106/KO15. *Cytogenet. Cell Genet.* **66**, 135–138. <https://doi.org/10.1159/000133685> (1994).
46. Liu, G., Maunoury, C., Kamoun, P. & Aral, B. Assignment of the human gene encoding the delta 1-pyrroline-5-carboxylate synthetase (P5CS) to 10q24.3 by in situ hybridization. *Genomics* **37**, 145–146. <https://doi.org/10.1006/geno.1996.0535> (1996).
47. Vékony, N., Wolf, S., Boissel, J. P., Gnauert, K. & Closs, E. I. Human cationic amino acid transporter hCAT-3 is preferentially expressed in peripheral tissues. *Biochemistry* **40**, 12387–12394. <https://doi.org/10.1021/bi011345c> (2001).
48. Rebsamen, M. *et al.* Gain-of-function genetic screens in human cells identify SLC transporters overcoming environmental nutrient restrictions. *Life Sci. Alliance* <https://doi.org/10.26508/lsa.202201404> (2022).
49. Cruzen, M. E., Bengtsson, U., McMahon, J., Wasmuth, J. J. & Arfin, S. M. Assignment of the cysteinyl-tRNA synthetase gene (CARS) to 11p15.5. *Genomics* **15**, 692–693. <https://doi.org/10.1006/geno.1993.1128> (1993).
50. Cahill, K. M., Huo, Z., Tseng, G. C., Logan, R. W. & Seney, M. L. Improved identification of concordant and discordant gene expression signatures using an updated rank-rank hypergeometric overlap approach. *Sci. Rep.* **8**, 9588 (2018).
51. Plaisier, S. B., Taschereau, R., Wong, J. A. & Graeber, T. G. Rank-rank hypergeometric overlap: Identification of statistically significant overlap between gene-expression signatures. *Nucleic Acids Res.* **38**, e169–e169 (2010).
52. Usoskin, D. *et al.* Unbiased classification of sensory neuron types by large-scale single-cell RNA sequencing. *Nat. Neurosci.* **18**, 145–153. <https://doi.org/10.1038/nn.3881> (2015).
53. Yang, L. *et al.* Human and mouse trigeminal ganglia cell atlas implicates multiple cell types in migraine. *Neuron* **110**, 1806–1821. e1808. <https://doi.org/10.1016/j.neuron.2022.03.003> (2022).
54. Wu, H. F. *et al.* Norepinephrine transporter defects lead to sympathetic hyperactivity in Familial Dysautonomia models. *Nat. Commun.* **13**, 7032. <https://doi.org/10.1038/s41467-022-34811-7> (2022).
55. Tolman, Z., Chaverra, M., George, L. & Lefcort, F. Elp1 is required for development of visceral sensory peripheral and central circuitry. *Dis. Model Mech.* **15**, dmm049274 (2022).
56. Leonard, C. E., Quiros, J., Lefcort, F. & Taneyhill, L. A. Loss of Elp1 disrupts trigeminal ganglion neurodevelopment in a model of familial dysautonomia. *Elife* **11**, e71455 (2022).
57. Matharu, N. & Ahituv, N. Modulating gene regulation to treat genetic disorders. *Nat. Rev. Drug Discov.* **19**, 757–775 (2020).
58. Gerasimavicius, L., Livesey, B. J. & Marsh, J. A. Loss-of-function, gain-of-function and dominant-negative mutations have profoundly different effects on protein structure. *Nat. Commun.* **13**, 3895 (2022).
59. Kojic, M. *et al.* A novel ELP1 mutation impairs the function of the Elongator complex and causes a severe neurodevelopmental phenotype. *J. Hum. Genet.* <https://doi.org/10.1038/s10038-023-01135-3> (2023).
60. Burgess, R. W. & Storkebaum, E. tRNA dysregulation in neurodevelopmental and neurodegenerative diseases. *Annu. Rev. Cell Dev. Biol.* **39**, 223–252 (2023).
61. Karlsborn, T., Tükenmez, H., Chen, C. & Byström, A. S. Familial dysautonomia (FD) patients have reduced levels of the modified wobble nucleoside mcm(5)s(2)U in tRNA. *Biochem. Biophys. Res. Commun.* **454**, 441–445. <https://doi.org/10.1016/j.bbrc.2014.10.116> (2014).
62. Frohloff, F., Jablonowski, D., Fichtner, L. & Schaffrath, R. Subunit communications crucial for the functional integrity of the yeast RNA polymerase II elongator (γ -toxin target (TOT)) complex. *J. Biol. Chem.* **278**, 956–961 (2003).
63. Dietrich, P., Alli, S., Shanmugasundaram, R. & Dragatsis, I. IKAP expression levels modulate disease severity in a mouse model of familial dysautonomia. *Hum. Mol. Genet.* **21**, 5078–5090. <https://doi.org/10.1093/hmg/dds354> (2012).
64. Dietrich, P., Yue, J., Shuyu, E. & Dragatsis, I. Deletion of exon 20 of the familial dysautonomia gene *Ikbk* in mice causes developmental delay, cardiovascular defects, and early embryonic lethality. *PLoS One* **6**, e27015 (2011).
65. Dobin, A. *et al.* STAR: Ultrafast universal RNA-seq aligner. *Bioinformatics* **29**, 15–21. <https://doi.org/10.1093/bioinformatics/bts635> (2013).
66. Bolger, A. M., Lohse, M. & Usadel, B. Trimmomatic: A flexible trimmer for Illumina sequence data. *Bioinformatics* **30**, 2114–2120. <https://doi.org/10.1093/bioinformatics/btu170> (2014).
67. Anders, S., Pyl, P. T. & Huber, W. HTSeq—A Python framework to work with high-throughput sequencing data. *Bioinformatics* **31**, 166–169. <https://doi.org/10.1093/bioinformatics/btu638> (2015).
68. Love, M. I., Huber, W. & Anders, S. Moderated estimation of fold change and dispersion for RNA-seq data with DESeq2. *Genome Biol.* **15**, 550. <https://doi.org/10.1186/s13059-014-0550-8> (2014).
69. Leek, J. T. svaseq: Removing batch effects and other unwanted noise from sequencing data. *Nucleic Acids Res.* **42**, e161. <https://doi.org/10.1093/nar/gku864> (2014).
70. Doncheva, N. T., Morris, J. H., Gorodkin, J. & Jensen, L. J. Cytoscape StringApp: Network analysis and visualization of proteomics data. *J. Proteome Res.* **18**, 623–632. <https://doi.org/10.1021/acs.jproteome.8b00702> (2019).
71. Shannon, P. *et al.* Cytoscape: A software environment for integrated models of biomolecular interaction networks. *Genome Res.* **13**, 2498–2504. <https://doi.org/10.1101/gr.1239303> (2003).
72. Subramanian, A. *et al.* Gene set enrichment analysis: A knowledge-based approach for interpreting genome-wide expression profiles. *Proc. Natl. Acad. Sci. USA* **102**, 15545–15550. <https://doi.org/10.1073/pnas.0506580102> (2005).
73. Langfelder, P. & Horvath, S. WGCNA: An R package for weighted correlation network analysis. *BMC Bioinform.* **9**, 559. <https://doi.org/10.1186/1471-2105-9-559> (2008).
74. Cortal, A., Martignetti, L., Six, E. & Rausell, A. Gene signature extraction and cell identity recognition at the single-cell level with Cell-ID. *Nat. Biotechnol.* **39**, 1095–1102. <https://doi.org/10.1038/s41587-021-00896-6> (2021).
75. Hao, Y. *et al.* Integrated analysis of multimodal single-cell data. *Cell* **184**, 3573–3587. e3529. <https://doi.org/10.1016/j.cell.2021.04.048> (2021).
76. Hafemeister, C. & Satija, R. Normalization and variance stabilization of single-cell RNA-seq data using regularized negative binomial regression. *Genome Biol.* **20**, 296 (2019).

Acknowledgements

We thank Dr. Alejandra Gonzalez-Duarte and Dr. Horacio Kaufmann of the Dysautonomia Treatment and Evaluation Center at New York University Medical School for their long-standing collaboration and helpful discussions. We are also grateful to Drs. Ioannis Dragatsis and Paula Dietrich at the University of Tennessee for the gift of the $Elp1^{fllox/+}$ and $Elp1^{\Delta20/+}$ mice and their collaborative effort to generate the FD phenotypic mouse model. This work was supported by National Institutes of Health (NIH) grants (R37NS095640 to S.A.S.) and by the HMS Ruth and Maurice Freeman Award for Pain Research (to E.M.).

Author contributions

R.S.H.: Conceptualization, Methodology, Software, Formal analysis, Writing—Original draft. E.M.: Conceptualization, Methodology, Validation, Formal analysis, Investigation, Writing—Original draft. M.S.: Investigation, Writing—Review and Editing. E.L.: Investigation. E.G.K.: Investigation. J.B.: Investigation. A.C.: Data curation, Investigation. B.C.: Data Curation, Methodology. R.Y.: Methodology, Writing—Review and Editing. S.E.: Methodology, Writing—Review and Editing. M.E.T.: Conceptualization, Supervision, Writing—Review and Editing. D.G.: Conceptualization, Supervision, Writing—Review and Editing. S.S.: Conceptualization, Supervision, Writing—Review and Editing, Funding acquisition.

Funding

NIH R37NS095640 to S.A.S. and HMS Ruth and Maurice Freeman Award for Pain Research to E.M.

Competing interests

The authors declare no competing interests. Susan A. Slaughaupt is a paid consultant to PTC Therapeutics and is an inventor on several U.S. and foreign patents and patent applications assigned to the Massachusetts General Hospital, including U.S. Patents 8,729,025 and 9,265,766, both entitled “[Methods for altering mRNA splicing and treating familial dysautonomia by administering benzyladenine](#),” filed on August 31, 2012 and May 19, 2014 and related to use of kinetin; and U.S. Patent 10,675,475 entitled, “[Compounds for improving mRNA splicing](#)” filed on July 14, 2017 and related to use of BPN-15477. Elisabetta Morini, Dadi Gao, Michael E. Talkowski and Susan A. Slaughaupt are inventors on an International Patent Application Number PCT/US2021/012103, assigned to Massachusetts General Hospital and entitled “[RNA Splicing Modulation](#)” related to use of BPN-15477 in modulating splicing.

Additional information

Supplementary Information The online version contains supplementary material available at <https://doi.org/10.1038/s41598-023-51137-6>.

Correspondence and requests for materials should be addressed to D.G. or S.S.

Reprints and permissions information is available at www.nature.com/reprints.

Publisher’s note Springer Nature remains neutral with regard to jurisdictional claims in published maps and institutional affiliations.



Open Access This article is licensed under a Creative Commons Attribution 4.0 International License, which permits use, sharing, adaptation, distribution and reproduction in any medium or format, as long as you give appropriate credit to the original author(s) and the source, provide a link to the Creative Commons licence, and indicate if changes were made. The images or other third party material in this article are included in the article’s Creative Commons licence, unless indicated otherwise in a credit line to the material. If material is not included in the article’s Creative Commons licence and your intended use is not permitted by statutory regulation or exceeds the permitted use, you will need to obtain permission directly from the copyright holder. To view a copy of this licence, visit <http://creativecommons.org/licenses/by/4.0/>.

© The Author(s) 2024, corrected publication 2024